Appl. Phys. B (2017) 123:70
DOI 10.1007/s00340-017-6646-6

Applied Physics B
Lasers and Optics

Directional energy focusing on monolayer graphene coupling system

Buzheng Wei[1,2] · Yuguang Yang[1,2] · Shuzhi Yao[1,2] · Han Xiao[1,2] · Shuisheng Jian[1,2]

Received: 3 December 2016 / Accepted: 13 January 2017 / Published online: 25 February 2017
© Springer-Verlag Berlin Heidelberg 2017

Abstract A directional energy focusing system based on parallel-monolayer graphene sheets is proposed and is analytically and numerically investigated in this paper. By properly designing the chemical potential distributions, we obtain a ~0.8-nm-size focusing point at desired positions with energy enhancement factor of over 2410. The flexible tunability of the transmission properties enables us to shut one parallel pair propagation down and guide the waves to the other branch. The light signal at the focal point is efficiently slowed down to over 10,000 times the speed in vacuum as well. The proposed structure may find potential applications in integrated circuits, on-chip systems or energy storage.

1 Introduction

Graphene is well known as a two-dimensional material, which is composed of a single layer of carbon atoms arranged in honeycomb lattices [1]. Since the emergence of graphene-based metamaterials [2], it has attracted intensive interests in the design of building plasmonic devices [3]. Surface plasmons polaritons (SPPs) are the collective oscillation of electrons located at the metal/dielectric interfaces [4], supporting travelling surface waves with strongly confined plasmon field beyond diffraction limit [5]. Compared to the SPPs on metal surface, graphene plasmons (GPs) have shown many superior properties, such as the strong field confinement [6] and the unique in situ tunability [7]. In particular, its gate voltage-dependent optical feature that the chemical potential of graphene can be tuned by means of external gate voltages [8, 9], allows for unprecedented tunability of electromagnetic structures made of graphene. It has been verified both theoretically and experimentally, and opens up an opportunity to electrically control plasmonic devices [10].

Intensive investigations on the graphene plasmonic devices such as waveguides [11], sensors [12], modulators [13] and optical switches [14] have been in the near-infrared regions, mid-infrared regions or beyond. Studies on the excitation of graphene plasmonic waves [15] give a perspective view on how to efficiently satisfy the resonant condition to design integrated resonant-induced graphene plasmonic device. By designing a grating substrate under the monolayer graphene sheet [16], resonant guide modes are sufficiently excited and two transmission dips appear in the total transmission region. Accompanied with a relatively larger propagation constant, the slow light effect is always achieved [17] in such structures. Among these previous works, energy focusing based on monolayer graphene have attracted our attention. Up to date, numerical investigations on nano-energy-focusing of electromagnetic waves have been reported both theoretically and experimentally. In a simple high-index dielectric nanoparticle-based conventional tapered plasmonic waveguide, Ref. [18] reported that the submicron-short-range SPPs waves have been successfully enhanced. By using the volume integral equation method, the metal-coated dielectric probes of tilted conical shape in Ref. [19] were investigated for nanofocusing of SPPs. Furthermore, Chen et al. [20] proposed a split-wedge antenna which can tightly confine gap plasmons and

✉ Buzheng Wei
14111010@bjtu.edu.cn

1 Key Laboratory of All Optical Network and Advanced Telecommunication Network of EMC, Beijing Jiaotong University, Beijing 100044, China

2 Institute of Lightwave Technology, Beijing Jiaotong University, Beijing 100044, China

boosted the local optical field intensity in and around these opposing metallic wedge tips and the Raman enhancement factors exceeding 10^7 were observed. However, the former researches mostly concentrated on complicated metal or slit structures which are relatively hard to build in experiments. Motivated by the simple design of graphene-based devices and EM transmission properties, we use a compact and easily integrated parallel graphene sheets coupling system to build novel nanofocusing structures. The propagation constant is composed of the wave number part and the energy loss part. Luckily, the dielectric parameters of graphene is actively tuned by the chemical doping or external gating methods. Therefore, if we alternate the competition between these two parts along the propagation direction by designing the desired eigenvalue for electromagnetic wave equations, the energy focusing effect can be actively controlled to our acknowledgement. Hence, we introduce a novel way proposed in Ref. [21] as our foundations to design our directional energy focusing system.

In this paper, we first analytically investigate the propagation constant and the transmission properties in Sect. 2. Numerical simulations about the way of giving higher coupling efficiency and basic directional focusing model are presented in Sect. 3. In this section, we successfully achieve energy directional focusing by applying the sharp decreasing chemical potential distribution functions to the secondary sheets. Next in Sect. 4, we explore the applications that can use such energy directional focusing mechanism. By varying the overlapped length or separation distance, we can achieve one-port focusing. The light trapped in the focal point can also be slowed down to over 10,000 times the speed in vacuum which give a way for energy storage on nano-chip system. The conclusions are drawn in Sect. 5.

2 Monolayer graphene directional coupling and energy focusing system

The schematic diagram of the proposed monolayer graphene directional energy focusing system is illustrated in Fig. 1. The overlapped length at the right end of the primary graphene sheet with the secondary sheet is set to be L nm. The distance between the parallel sheets is d nm. The incident wave impinges on the left port of the primary graphene sheet with magnetic field component perpendicular to the propagation direction. Since the thickness of the graphene layer is modeled here as $\Delta = 0.5$ nm which is extremely small compared to the wavelength, the sheet can be treated as zero thickness and still yields similar propagation properties in terms of the following analytical and numerical investigations. The configuration is z direction infinite and y direction zero thickness. Thus, only surface current exists as $J = \sigma_s E$ and no current in y direction. σ_s is

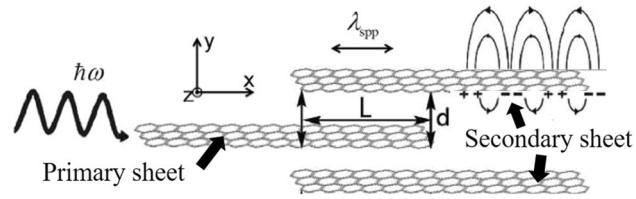

Fig. 1 The schematic diagram of the directional energy focusing system. The overlapped length is L nm, the distance between the primary and the secondary sheet is d nm

the surface conductivity of graphene. The graphene is surrounded by air and it is itself the boundary. The non-zero components of the electromagnetic field are H_z, E_x, E_y. The electrical field component perpendicular to the graphene sheet E_y, is discontinuous and anti-phase, while E_x parallel to graphene is continuous and in-phase, and H_z is also discontinuous due to the existence of the surface current [21]. The whole system contains two significant transmission mechanisms. First, for the single-layer region surrounded by air, the wave vector β of the SPP wave is given by [22]

$$\beta = k_0\sqrt{1-(2/\eta_0\sigma_s)^2}, \tag{1}$$

where $k_0 = 2\pi/\lambda$ is the wave number in vacuum. $\eta_0 = 377\,\Omega$ denotes the impedance of the air. Second, for the overlapped region also surrounded by air, the wave vector is obtained by [23]

$$\beta_\pm = \beta + \frac{2ik_0/(\eta_0\sigma_s) - k_p(1\mp u_p)}{(1\mp u_p)\beta/k_p \pm u_p\beta d}, \tag{2}$$

where β_+ and β_- stand for the symmetric and antisymmetric SPP modes supported by the overlapped parallel graphene sheets, $k_p = (\beta^2 - k_0^2)^{1/2}$ and $u_p = \exp(-k_p d)$. Obviously, the SPP wave propagates to the end of the primary graphene sheet and couples energy into the secondary one. With proper design of the overlapped length, the maximum coupling coefficient and transmission coefficient can be obtained. Anyway, the purpose of the structure is not to realize the energy coupling, but to realize the energy switch focusing. Hence, we virtually vary the chemical doping or external gating of the secondary graphene sheet in such way, that the coupled energy on the secondary graphene monolayer will be focused to the desired positions. Thus, the so-called directional energy focusing can be actively achieved.

One way to realize energy focusing is to adjust the relationship between the wave number and transmission loss. As derived from Eq. (1), β can be described as $\beta = \mathrm{Re}(\beta) + i\mathrm{Im}(\beta)$, where $\mathrm{Re}(\beta)$ and $\mathrm{Im}(\beta)$ represent the wave number and transmission loss, respectively. If $\mathrm{Im}(\beta)$ is considerably small, it means the SPP wave can travel to the end of the sheet without much energy loss. In addition,

if the wave number is quite large at one point, the competition between energy saving and losing swings to the former one, which means an energy enhancing point is thus created here. To extreme extensions when Re(β) is infinite, the effective refractive index is infinite as well. In such condition, the group velocity of the SPP wave shrinks to zero. The light propagating to this point is trapped and cannot get out anymore. However, such conditions are not practical. But we can design the loss rate far exceeding the energy saving speed beyond that point, which also builds a transmission stop point under practical conditions. Our structure uses this method to realize energy switch focusing. Combined with the directional coupling, we can focus energy to either the upper sheet or the lower sheet like an optical switch or splitter.

3 Numerical simulations of the basic energy directional focusing structure

To verify the ideas of the proposed energy switch focusing system, we numerically investigate the possibilities using finite element methods (FEM) with our COMSOL software Ver 5.2. To start with, we have to give the material properties for our simulations. The only material property we use here is the relative permittivity tensors of graphene. The simulated frequency region covers the mid-infrared band, so the effect from interband electron transition cannot be neglected. As mentioned above, the conductivity of graphene is the surface conductivity. Hence, σ_s can be expressed as $\sigma_s = \sigma_{\text{inter}} + \sigma_{\text{intra}}$ [21], where σ_{inter} denotes the interband transition contribution which can be given by [24]

$$\sigma_{\text{inter}} = i\frac{e^2}{4\pi\hbar}\ln\left[\frac{2|\mu_c| - \hbar(\omega + i\tau^{-1})}{2|\mu_c| + \hbar(\omega + i\tau^{-1})}\right], \tag{3}$$

here e is the electron charge, μ_c is the chemical potential of graphene, $\hbar$ is the reduced Planck constant, ω is the incident angular frequency in vacuum and τ is the momentum relaxation time due to charge carrier scattering. σ_{intra} corresponds to the intraband electron–photon scattering and is derived by [24]

$$\sigma_{\text{intra}} = i\frac{e^2 k_B T}{\pi\hbar^2(\omega + i\tau^{-1})}\ln\left[\frac{\mu_c}{k_B T} + 2\ln\left(\exp\left(-\frac{\mu_c}{k_B T}\right) + 1\right)\right], \tag{4}$$

where k_B is the Boltzmann constant and T is the temperature. The graphene film is modeled as a thin layer and an anisotropic dielectric constant described by a diagonal tensor [15]. The surface relative permittivity of graphene is denoted by $\epsilon_{xx} = \epsilon_{zz} = 2.5 + i\sigma_s/\epsilon_0\omega\Delta$ and the surface normal component is $\epsilon_{yy} = 2.5$ based on the dielectric constant of graphite [15]. Throughout this paper we use a conservative $\tau = 0.5$ ps and set $T = 300$ K. The chemical potential distributions for the primary and secondary graphene sheets are different which will be given on certain circumstances next.

The primary graphene monolayer is set at $x = 0$ nm, $y = 0$ nm with the length of 1000 nm. Here we only build the upper sheet for simplicity, the same mechanism can be applied when the lower is built as well. The chemical potential is 0.4 eV here for both the primary and the secondary graphene sheet in order to choose a moderate value for the overlapped length L and the distance d. The incident light frequency is $f = 50$ THz. The transmission which is defined by the S-parameters as a function of the overlapped length L and the distance d is depicted in Fig. 2. From the figure we can conclude that when $L = 150$ nm and $d = 75$ nm, the transmission is relatively high. Without the wave vector designing we discussed in Sect. 2, the SPP wave is successfully coupled to the secondary graphene sheet and the output power is 0.49 times the input one. The z component of magnetic field (H_z) distribution is shown in Fig. 2b, c for the highest and lowest transmission, respectively. It should be emphasized here that the smaller separation distance d is, the stronger coupling effect it presents. The purpose we need to focus is not to find the highest transmission point in this paper, but to realize energy directional

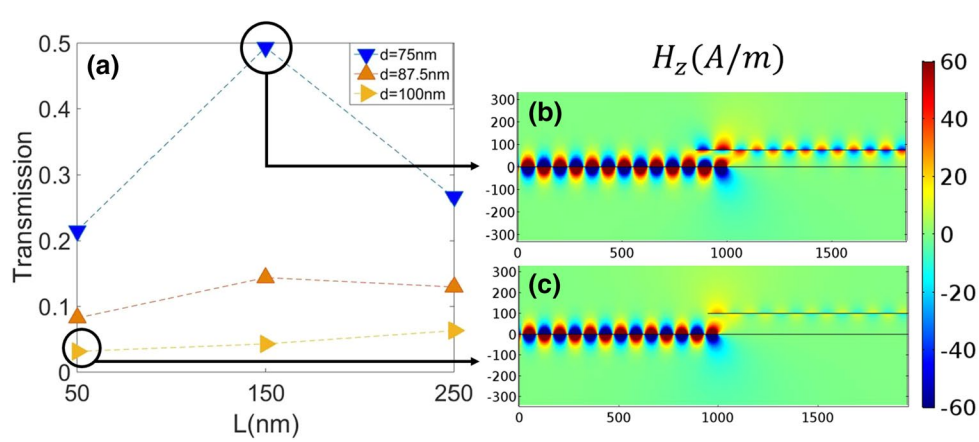

Fig. 2 **a** The transmission as a function of L and d under incident frequency $f = 50$ THz. The H_z distributions of **b** $L = 150$ nm, $d = 75$ nm and **c** $L = 50$ nm, $d = 100$ nm. The transmission coefficients are 0.49 and 0.03, correspondingly

focusing. So the values we choose for L and d are acceptable based on the research in [25]. The SPP mode confined tightly to the surface of the graphene sheet is guided along the propagation direction and presents periodically alternative positive–negative value. Due to the superposition of antisymmetric mode in the overlapped region as in Fig. 2c, some low couplings appear.

Next, we virtually create a sharp changing chemical potential distributions on the secondary graphene sheet to realize energy focusing. Despite the uniformly distributed chemical potential 0.4 eV in Fig. 2, we give the distribution function as follows according to [21]

$$\mu_c = \mu_{c0}[1 - \exp(0.015(x - 1750))], \quad (5)$$

where $\mu_{c0} = 0.4$ eV is the chemical potential at the left port of the secondary graphene sheet and x stands for the x coordinate according to which the secondary sheet is located. It has been reported that a linear chemical distribution was realized in Ref. [26]. Besides, a high-mobility and high-purity graphene monolayer is experimentally demonstrated to realize ultrafast optical switching by modulating the chemical potential of graphene [27]. The distributions here ensure a rapid μ_c decrement around $x = 1700$ nm resulting in a rapid increment in both $\mathrm{Re}(\beta)$ and $\mathrm{Im}(\beta)$. Here, we define the point where $\mathrm{Re}(\beta) = \mathrm{Im}(\beta)$ is the critical point. Around this point, $\mathrm{Im}(\beta)$ increases drastically from an extremely small value to far exceeding $\mathrm{Re}(\beta)$. Thus, when a single frequency incident wave propagates along the secondary sheet to closely before the critical point where $\mathrm{Re}(\beta) \gg \mathrm{Im}(\beta)$, energy will be efficiently focused. Once beyond the critical point, the energy loss begins to dominate, which gives a sharp termination to the propagation of the SPP wave. Here, we give the upper and the lower sheet the same distribution function. The normalized electric field distribution and the z component magnetic field distribution of the energy focusing switch system is illustrated in Fig. 3b, c. From the numerical results, we can clearly recognize the sharp ending of energy flow along the secondary graphene sheet. The energy intensity enhancement factor is defined as $R = |E_{\mathrm{peak}}|^2/|E_{1100}|^2$, where $|E_{1100}|$ is the norm of electric field at $x = 1100$ nm. Since the wave in the overlapped region splits into two modes and the amplitude is the superposition of the symmetric and antisymmetric modes, we cannot use the norm electric field at the left coupling port to normalize the $|E_{\mathrm{peak}}|$. Therefore, when the SPP waves travel beyond the coupling region, the values of norm electric field are from one single SPP mode and are appropriate to take for the normalization coefficient. It should be pointed out that $|E_{1100}|$ is not a special value we must choose for the normalization coefficient as long as the value is slightly beyond the coupling region and pronounces the feasibility. The values of $|E|/|E_{1100}|$ along $y = 75.75$ nm, $x = 1700$–1750 nm under different incident frequencies are plotted in Fig. 3a. From the numerical calculations, the highest R reaches 2410 under incident frequency $f = 45$ THz and the full width at half maximum (FWHM) of which is 0.8 nm. It is obvious that other frequencies have the same order of magnitude spot sizes. The focal points distinguish from each other along x axis, which gives a way for signal position control composed of multi-frequency. The reason for this phenomenon can also be explained as when the SPP wave does not reach the focusing point, the local chemical potential is far above $\hbar\omega/2$. σ_{inter} has a small real part and the loss is dominated by intraband electron–photon scattering, thereby bringing very limited loss to the propagation of SPP waves [21]. However, when the chemical potential continues decreasing and reaches around $\hbar\omega/2$, the contribution of loss from interband electron transition becomes more significant and eventually dwarfs the counterpart from intraband electron–photon scattering, rendering the SPP waves to vanish [21].

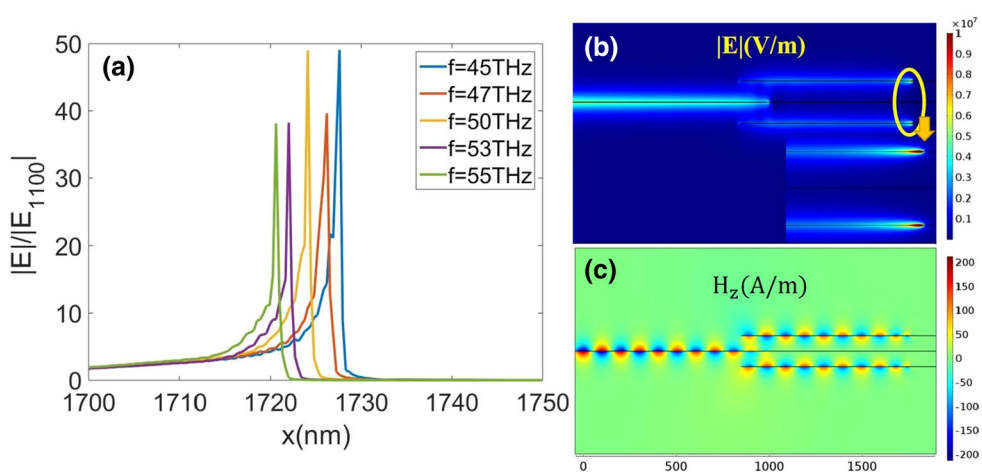

Fig. 3 **a** The $|E|/|E_{1100}|$ along *x axis*. **b** The norm electric field $|E|$ distribution for incident frequency $f = 45$ THz. The magnification of **b** shows the energy focusing effect at $x = 1728$ nm. Beyond that point, the propagation of the SPP wave is terminated. **c** The H_z distribution is in accordance with the $|E|$ distribution, a sharp ending is at $x = 1728$ nm

4 Directional energy focusing applications

The flexible switching properties enable us to design practical energy switch focusing devices based on the previous analytical and numerical investigations. The significant advantage of monolayer graphene is in its unique tunability of chemical potential control. By chemical doping or external gating, the local chemical potential can be changed instead of the uniformly chemical potential distribution. Rather than the identical chemical potential distribution function we use in Sect. 3 for both the upper and the lower sheets, we modify the lower sheet's chemical potential distribution function to

$$\mu_{cl} = \mu_{c0}[1 - \exp(0.025(x - 1550))], \quad (6)$$

where the changes are the migration of critical point position from around $x = 1700$ nm to $x = 1500$ nm and the decreasing rate from 0.015 to 0.025. Different from the same propagation in Fig. 3, the SPP waves propagating along the lower sheet terminate at around $x = 1500$ nm. The $|E|$ and H_z distributions are plotted in Fig. 4. In this way, the energy can be focused at the desired working regions switched by the system. The device is composed of three parallel-monolayer graphene sheets and can be conveniently integrated into the nano-structure devices as a light source for different subsystem.

A more typical use of the optical switch is to shut one parallel pair propagation down and guide the SPP wave to the other pair. From the discussion above about the coupling efficiency shown in Fig. 2a, we can vary the overlapped length L and the distance d to realize the shut down effect. For convenience, now we distinguish that L_1 and L_2 stand for the overlapped length for the upper and lower sheets, respectively. The same principle is applied for d_1 and d_2. First, we hold $d_1 = d_2 = 75$ nm and decrease $L_1 = 50$ nm while $L_2 = 150$ nm. Apparently, the energy enhancement effect of the upper pair is relatively reduced as illustrated in Fig. 5c. Yet, there still remains coupling energy on the upper pair. Then, we hold $L_1 = L_2 = 150$ nm and pull away the upper pair to $d_1 = 100$ nm while $d_2 = 75$ nm. The energy accumulated by the upper sheet is largely reduced, too, as shown in Fig. 5f. The corresponding field distributions are depicted in Fig. 5a, b, d, e as well. Although the energy focused in one pair is largely reduced, we still need to eliminate the focusing effect completely. As comparison, we delete the chemical distribution function used for the upper sheet and use the uniformly distribution of 0.1 eV. The energy is completely guide to the lower sheet at last. The field distributions are plotted in Fig. 6.

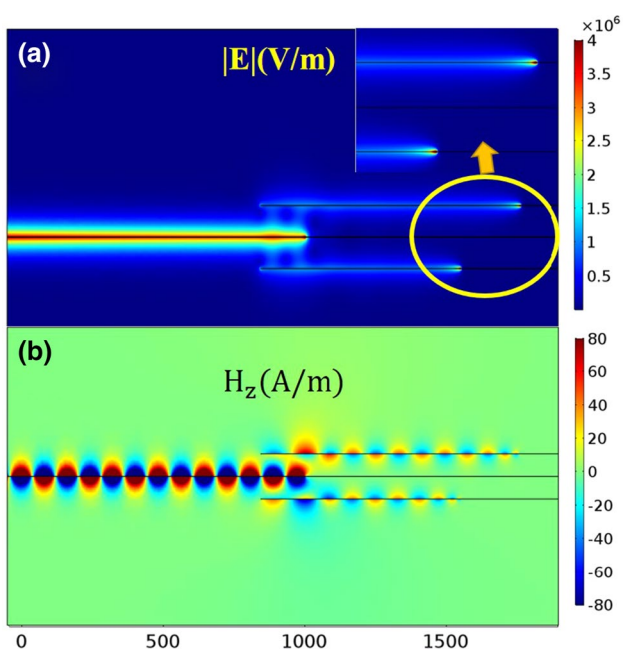

Fig. 4 The **a** $|E|$ and **b** H_z distributions for incident frequency $f = 50$ THz. The magnification of **a** shows the energy focusing effect at different positions along the two secondary graphene sheets. Beyond that point, the propagation of the SPP wave is terminated

The applications of the proposed device not only contain optical switching effect, but also the slow light effect. It is known that the light propagates in dielectric medium with the refractive index n will have group velocity $v_g = c/(n + \omega dn/d\omega)$ and group index $n_g = c/v_g$ [17]. c is the velocity of light in vacuum. According to Eq. (1), the effective refractive index of the monolayer graphene is obtained by $n_{eff} = \mathrm{Re}(\beta)/k_0$. According to Eqs. (3) and (4), the surface conductivity is a function of incident frequency and chemical potential. Thus, first we hold $\mu_c = 0.2$ eV and plot n_g and $\mathrm{Re}(\beta) - \mathrm{Im}(\beta)$ as a function of incident frequency in Fig. 7a. From the figure we can see that when $f < 80$ THz, $\mathrm{Re}(\beta) > \mathrm{Im}(\beta)$ and n_g remains low. When the frequency continues to increase to very close to 80 THz, the group index n_g increases drastically to over 4000 because $\mathrm{Re}(\beta)$ gets larger. Once beyond 80 THz, $\mathrm{Re}(\beta) < \mathrm{Im}(\beta)$ causing the propagation to terminate and the group index decreases sharply. Therefore, if the incident wave contains multiple frequency components, certain frequency component will be focused to the corresponding position just ahead of where $\mathrm{Re}(\beta) = \mathrm{Im}(\beta)$. Meanwhile, the group index here is a relatively large value causing the light to slowdown. The best slowdown occurs in Fig. 7b with n_g over 10,000 when $\mu_c = 0.5$ eV and $f = 200$ THz. Next we hold the incident frequency $f = 50$ THz and plot n_g and $\mathrm{Re}(\beta) - \mathrm{Im}(\beta)$ as a function of μ_c. Similar to the first circumstance, when μ_c increases to approximately 0.2 eV, $\mathrm{Re}(\beta) < \mathrm{Im}(\beta)$ causing the light to stop propagating. Closely before that point, n_g comes to a increasingly high value causing the light to slowdown. For different incident frequency components, certain component finds the corresponding critical μ_c and the energy is stored here with

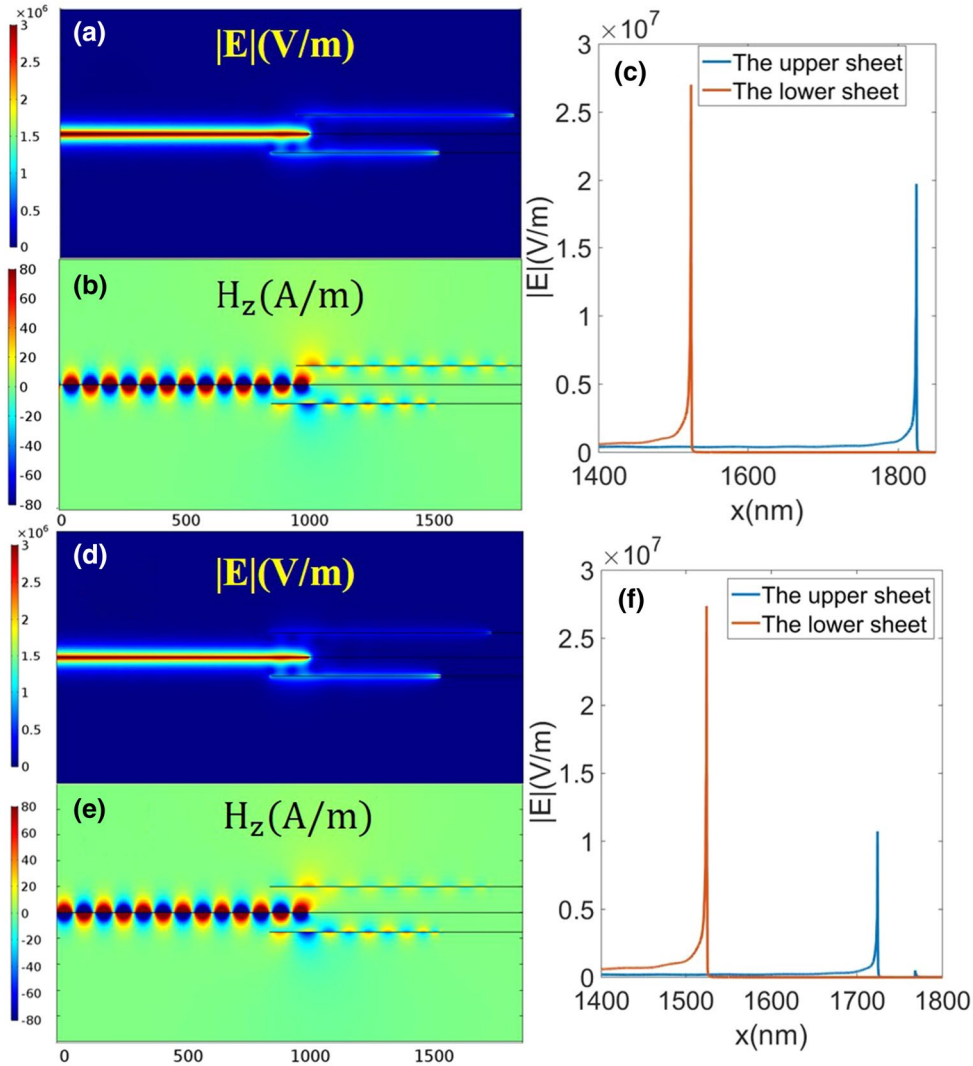

Fig. 5 The **a** $|E|$ and **b** H_z distributions for incident frequency $f = 50$ THz under $L_1 = 50$ nm, $L_2 = 150$ nm and $d_1 = d_2 = 75$ nm. **c**, **f** The value of $|E|$ along *x axis* from the *y axis* center of the upper and lower sheets. The **d** $|E|$ and **e** H_z distributions for incident frequency $f = 50$ THz under $L_1 = L_2 = 150$ nm and $d_1 = 100$ nm, $d_2 = 75$ nm

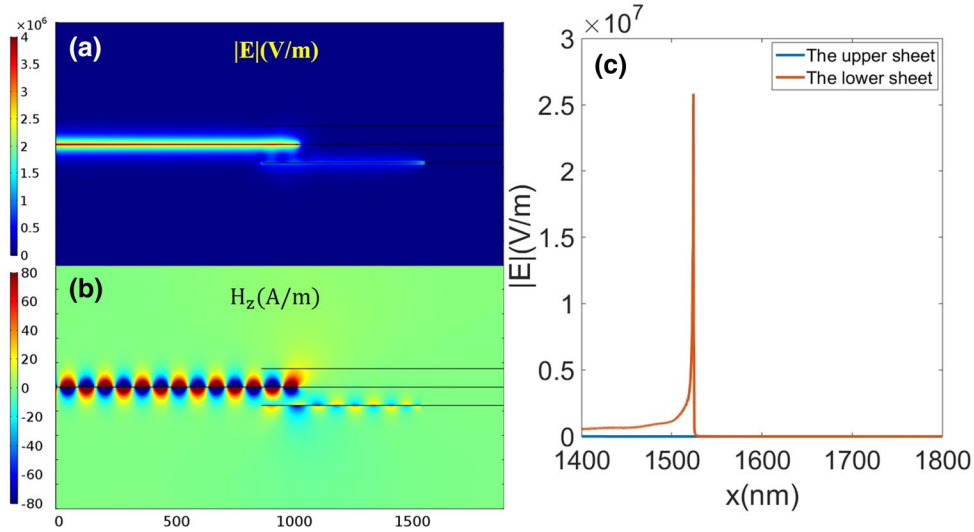

Fig. 6 The **a** $|E|$ and **b** H_z distributions for incident frequency $f = 50$ THz under $L_1 = L_2 = 150$ nm and $d_1 = d_2 = 75$ nm. Only the lower sheet is applied with the chemical potential distribution function, the upper sheet is uniformly 0.1 eV. **c** The value of $|E|$ along *x axis* from the *y axis* center of the upper and lower sheets

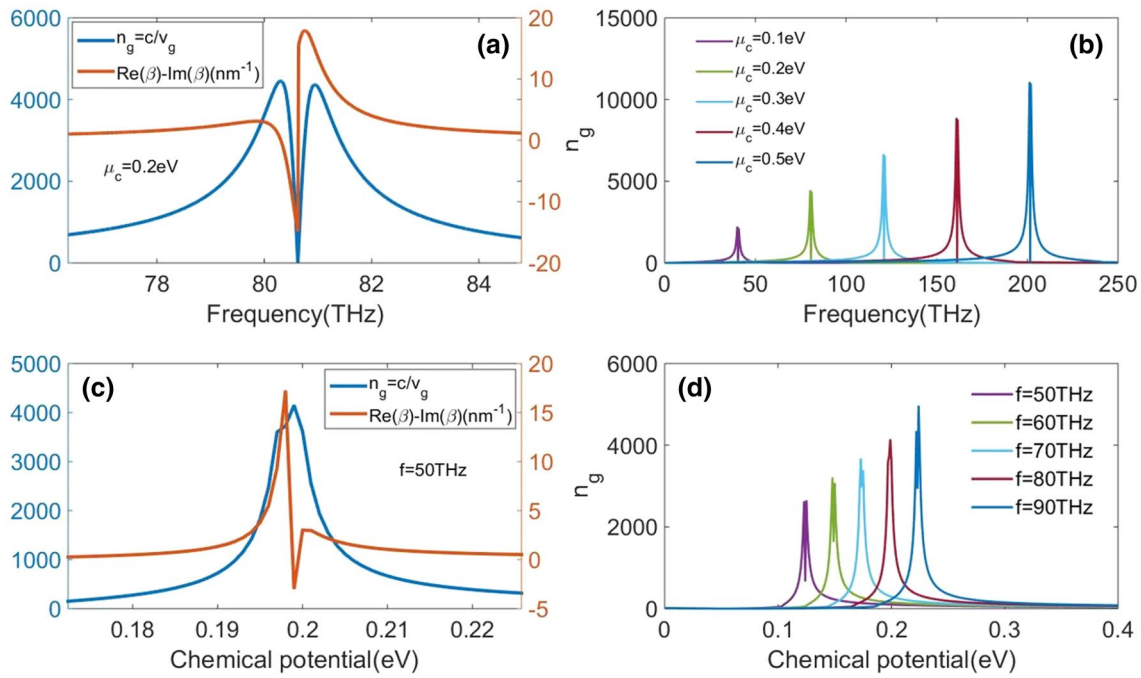

Fig. 7 **a** n_g and $\mathrm{Re}(\beta) - \mathrm{Im}(\beta)$ as a function of incident frequency when $\mu_c = 0.2$ eV. **b** n_g as a function of incident frequency under different μ_c. **c** n_g and $\mathrm{Re}(\beta) - \mathrm{Im}(\beta)$ as a function of chemical potential when $f = 50$ THz. **d** n_g as a function of chemical potential under different incident frequencies

a large group index. The best slowdown occurs in Fig. 7d with n_g over 5000 when $\mu_c = 0.23$ eV and $f = 90$ THz.

The whole structure is very simple to fabricate and easy to change the chemical potential distributions of graphene. However, the main drawback is the difficulty to realize monolayer graphene sheet system. To our knowledge, most cases are on the silicon substrate and a metal electrode is extended outside to tune the gate voltages. The local chemical distributions is not ideally the design we virtually used in simulations. Yet, our device still gives a perspective for designing novel energy directional focusing systems.

5 Conclusion

In this paper, we analytically and numerically investigated a parallel-monolayer overlapped graphene system to realize energy directional focusing effect. First, we found the appropriate overlapped length and separation distance between the primary and the secondary sheet to realize relatively higher coupling efficiency. Then, by applying the sharp decreasing chemical potential distribution functions to the secondary sheets, we successfully achieved directional focusing at the desired positions on the secondary sheets. Furthermore, by exploring the overlapped length and separation distance, we obtained one-port focusing and shut down the other as well. The energy enhancement factor reached over 2410 and spot size of the focal point is of 0.8 nm order of magnitudes. In the end, the slowdown effect was analytically investigated and a group index of over 10,000 was presented. The proposed ideas may find potential applications in integrated circuits or on-chip systems.

Acknowledgements This work was supported by the National Science Fund for Distinguished Young Scholars Grant No. 61525501.

References

1. K.S. Novoselov, A.K. Geim, S.V. Morozov, D. Jiang, M.I. Katsnelson, I.V. Grigorieva, S.V. Dubonos, A.A. Firsov, Two-dimensional gas of massless dirac fermions in graphene. Nature **438**(7065), 197–200 (2005)
2. A.K. Geim, K.S. Novoselov, The rise of graphene. Nat. Mater. **6**(3), 183–191 (2007)
3. A.N. Grigorenko, M. Polini, K.S. Novoselov, Graphene plasmonics. Nat. Photon. **6**(11), 749–758 (2012)
4. J. M. Pitarke, V. M. Silkin, E. V. Chulkov, P. M. Echenique, Theory of surface plasmons and surface-plasmon polaritons. Physics
5. D.K. Gramotnev, S.I. Bozhevolnyi, Plasmonics beyond the diffraction limit. Nat. Photon. **4**(2), 83–91 (2010)
6. A. Vakil, N. Engheta, Transformation optics using graphene. Science (New York, N.Y.) **332**(6035), 1291–1294 (2011)
7. F. Xia, H. Wang, D. Xiao, M. Dubey, A. Ramasubramaniam, Two-dimensional material nanophotonics. Nat. Photon. **8**(12), 899–907 (2014)

8. J. Chen, M. Badioli, P. Alonso-Gonzalez, S. Thongrattanasiri, F. Huth, J. Osmond, M. Spasenovic, A. Centeno, A. Pesquera, P. Godignon, A. Zurutuza Elorza, N. Camara, F.J.G. de Abajo, R. Hillenbrand, F.H.L. Koppens, Optical nano-imaging of gate-tunable graphene plasmons. Nature **487**(7405), 77–81 (2012)
9. Z. Fei, A.S. Rodin, G.O. Andreev, W. Bao, A.S. McLeod, M. Wagner, L.M. Zhang, Z. Zhao, M. Thiemens, G. Dominguez, M.M. Fogler, A.H.C. Neto, C.N. Lau, F. Keilmann, D.N. Basov, Gate-tuning of graphene plasmons revealed by infrared nano-imaging. Nature **487**(7405), 82–85 (2012)
10. H.-J. Li, X. Zhai, B. Sun, Z.-R. Huang, L.-L. Wang, A graphene-based bandwidth-tunable mid-infrared ultra-broadband plasmonic filter. Plasmonics **10**(4), 765–771 (2015)
11. J.-P. Liu, X. Zhai, L.-L. Wang, H.-J. Li, F. Xie, Q. Lin, S.-X. Xia, Analysis of mid-infrared surface plasmon modes in a graphene-based cylindrical hybrid waveguide. Plasmonics **11**(3), 703–711 (2016)
12. C. Chen, D. Zhao, T. Hu, J. Sun, X. Yang, Highly fluorescent nitrogen and sulfur co-doped graphene quantum dots for an inner filter effect-based cyanide sensor. Sens. Actuators B Chem. **241**, 779–788 (2017)
13. A.A. Sayem, M.R.C. Mahdy, I. Jahangir, M.S. Rahman, Ultrathin ultra-broadband electro-absorption modulator based on few-layer graphene based anisotropic metamaterial. Opt. Commun. **384**, 50–58 (2017)
14. Y. Li, H. Yu, T. Dai, J. Jiang, G. Wang, L. Yang, W. Wang, J. Yang, X. Jiang, Graphene-based floating-gate nonvolatile optical switch. IEEE Photon. Technol. Lett. **28**(3), 284–287 (2016)
15. W. Gao, J. Shu, C. Qiu, Q. Xu, Excitation of plasmonic waves in graphene by guided-mode resonances. ACS Nano **6**(9), 7806–7813 (2012)
16. B. Wei, H. Liu, G. Ren, Y. Yang, S. Ye, L. Pei, S. Jian, Graphene based silicon-air grating structure to realize electromagnetically-induced-transparency and slow light effect. Phys. Lett. A **381**(3), 160–165 (2017)
17. H. Lu, C. Zeng, Q. Zhang, X. Liu, M.M. Hossain, P. Reineck, M. Gu, Graphene-based active slow surface plasmon polaritons. Sci. Rep. **5**, 8443 (2015)
18. C.-C. Yu, K.-T. Lin, P.-Y. Su, E.-Y. Wang, Y.-T. Yen, H.-L. Chen, Short-range plasmonic nanofocusing within submicron regimes facilitates in situ probing and promoting of interfacial reactions. Nanoscale **8**, 3647–3659 (2016)
19. N.T. Thu, K. Tanaka, M. Tanaka, D.N. Chien, Superfocusing of surface plasmon polaritons by metal-coated dielectric probe of tilted conical shape. J. Opt. Soc. Am. A **30**(6), 1113–1118 (2013)
20. X. Chen, N.C. Lindquist, D.J. Klemme, P. Nagpal, D.J. Norris, S.-H. Oh, Split-wedge antennas with sub-5 nm gaps for plasmonic nanofocusing. Nano Lett. **16**(12), 7849–7856 (2016)
21. W. Qiu, X. Liu, J. Zhao, S. He, Y. Ma, J.-X. Wang, J. Pan, Nanofocusing of mid-infrared electromagnetic waves on graphene monolayer. Appl. Phys. Lett. **104**(4), 041109 (2014). doi: 10.1063/1.4863926
22. B. Wang, X. Zhang, X. Yuan, J. Teng, Optical coupling of surface plasmons between graphene sheets. Appl. Phys. Lett. **100**(13), 131111 (2012). doi: 10.1063/1.3698133
23. H.-J. Li, L.-L. Wang, B. Sun, Z.-R. Huang, X. Zhai, Controlling mid-infrared surface plasmon polaritons in the parallel graphene pair. Appl. Phys. Express **7**(12), 125101 (2014)
24. G.W. Hanson, Dyadic greens functions and guided surface waves for a surface conductivity model of graphene. J. Appl. Phys. **103**, 064302 (2008). doi: 10.1063/1.2891452
25. H. Li, L. Wang, Z. Huang, B. Sun, X. Zhai, X. Li, Mid-infrared, plasmonic switches and directional couplers induced by graphene sheets coupling system. Europhys. Lett. **104**(3), 37001 (2013)
26. W. Qiu, X. Liu, J. Zhao, Y. Huang, H. Chen, B. Li, J.-X. Wang, Q. Kan, J.-Q. Pan, Ultrabroad band rainbow capture and releasing in graded chemical potential distributed graphene monolayer. Plasmonics **10**(5), 1023–1028 (2015)
27. G.X. Ni, L. Wang, M.D. Goldflam, M. Wagner, Z. Fei, A.S. McLeod, M.K. Liu, E. Keilmann, B. Özyilmaz, H.A.C. Neto, J. Hone, M.M. Fogler, D.N. Basov, Ultrafast optical switching of infrared plasmon polaritons in high-mobility graphene. Nat. Photon. **10**(4), 244–247 (2016)